Tool Temperatures in Orthogonal Cutting of Alloyed Titanium

Robert W. Ivester
Engineering Laboratory
National Institute of Standards and Technology[1]
Gaithersburg, Maryland, USA

ABSTRACT
This paper presents infrared-based measurements and analysis of cutting tool temperatures for orthogonal machining of alloyed titanium. High-speed infrared video provided the basis for measurement of cutting tool temperature distribution as reported here for cutting speeds from 55 m/min to 125 m/min with tungsten carbide tooling with and without a titanium nitride coating. The presence of the coating provides a reduction in tool temperature of approximately 100 °C. Increasing the cutting speed from 55 m/min to 125 m/min increases the peak tool temperature by approximately 70 °C.

KEYWORDS
Infrared temperature measurement, Machining, Tungsten carbide, Titanium nitride, Tool coating, Cutting speed, Tool temperature.

INTRODUCTION

The technical and economic importance of metal cutting in general, and alloyed titanium in particular, provides a strong motivation for improving the scientific basis for understanding fundamental material and process behavior. Improvements in fundamental understanding of metal cutting provide industrial practitioners with a more meaningful basis for improving machining strategies, including tool path planning, cutting tool selection, and process parameter selection. Metal cutting can cause plastic deformation rates of 10^6 s^{-1}, thermal gradients of 10^3 °C/mm, heating rates of 10^6 °C/s, and contact pressures of 10^9 Pa. The ability to accurately model material plastic deformation under these conditions depends on accurate measurement of temperatures and temperature gradients in metal cutting.

The measurement uncertainty limitations for machining temperatures hinder the fidelity of models for a variety of performance measures of practical interest, including forces, tool wear, friction, geometric accuracy, residual stress, surface quality, subsurface damage, and burr formation [Komanduri 1993]. Each of these process performance measures strongly influences the cost and product performance of critical components in a variety of high-technology durable goods.

The history of temperature measurement techniques in metal cutting has been thoroughly reviewed [Stephenson and Agapiou 1997, Davies et al. 2007] and analyzed for relative strengths and limitations. Starting in the 1920's, the "intrinsic thermocouple" technique based on the inherent electromotive force created by the elevated temperature at the contact between the tool and the workpiece provided an effective relative indicator of rake face temperature [Boston and Gilbert 1935, Herbert 1926, Stephenson 1993, Trigger 1948]. The general trends of cutting temperatures measured through the intrinsic thermocouple technique with changes in tool geometry, cutting conditions, and material microstructure agree with extensive works investigating chip morphology, microstructure, and tool microstructure based on quick-stop devices and tool temperature measurements by embedded thermocouples [Stephenson and Agapiou 1997].

Pioneering efforts in infrared photography-based temperature measurement in metal cutting [Boothroyd 1961] provided useful insight into the spatial distribution of cutting tool temperatures. The limited sensitivity of the infrared-sensitive film required substantial preheating of the workpiece, and extremely long exposure times reduced the quantitative utility of the measurements. Recent advancements in digital infrared-sensitive detector arrays enable microsecond-level control of integration time and frame timing and provide dramatically improved sensitivity

[1] Commercial equipment is identified in order to adequately specify certain procedures. In no case does such identification imply recommendation or endorsement by the National Institute of Standards and Technology, nor does it imply that the materials or equipment are necessarily the best available for the purpose.

to infrared light [Aluwihare et al. 2000, Arrazola et al. 2008, Davies et al. 2003(1), Davies et al. 2003(2), Ivester et al. 2005, Whitenton et al. 2005, Whitenton 2010].

This paper presents the experimental setup, results, and analysis for temperature and force measurements during orthogonal cutting using infrared videography at 300 frames per second with a field of view approximately 1 mm wide and a 3-axis dynamometer. The experiments address the machining of alloyed titanium (Ti-6Al-4V) with uncoated and coated (TiN) tools at a +6 degree positive rake and 30 μm edge radius at cutting speeds ranging from 55 m/min to 125 m/min.

EXPERIMENTAL SETUP

A four-axis high-speed grinding machine provides a high stiffness experimental platform for the orthogonal cutting tests in this paper [Ivester et al. 2005]. A disk-shaped workpiece bolted to the horizontal spindle moves along a vertical axis towards a stationary cutting tool mounted on a 3-axis dynamometer on the machine table. Locating the cutting edge parallel to and directly under the spindle axis along the vertical axis of motion ensures an orthogonal cut. The horizontal spindle axis moves vertically and the tool remains stationary during the testing. Since the tool does not move during the cutting test, cameras mounted outside the machine tool can measure the machining process with minimal disturbance from machine tool vibrations. Grinding off the corner of the cutting insert provides a flat surface perpendicular to the cutting edge and enables camera-based measurement of the tool temperature distribution.

A high-magnification reflective lens and spectral beam splitter transmits infrared light into a high-speed infrared spectrum camera and reflects visible light into a high-speed visible spectrum camera. The visible spectrum video detects abnormalities in the process that can be difficult to diagnose with only the infrared camera, resulting in lower measurement uncertainty.

Obtaining repeatable temperature measurements requires adequate parallelism of the disk surfaces. The parallelism affects the location of the disk surface relative to the mounting surface (5 μm flatness) and the side of the chip being imaged. The workpiece preparation includes sawing oversized disks from 127 mm diameter bar stock, rough and finish turning of each side and drilling bolt holes to match the spindle mount. Subsequent grinding of both sides of the disk ensures flatness and parallelism to within 50 μm. Figures 1 and 2 present representative examples of video frames from the visible and infrared spectrum cameras, respectively. The sides of the tool, the chip, and the workpiece are approximately co-planar, but only the tool appears to be in focus because the chip and workpiece both move significantly during acquisition of the video frame.

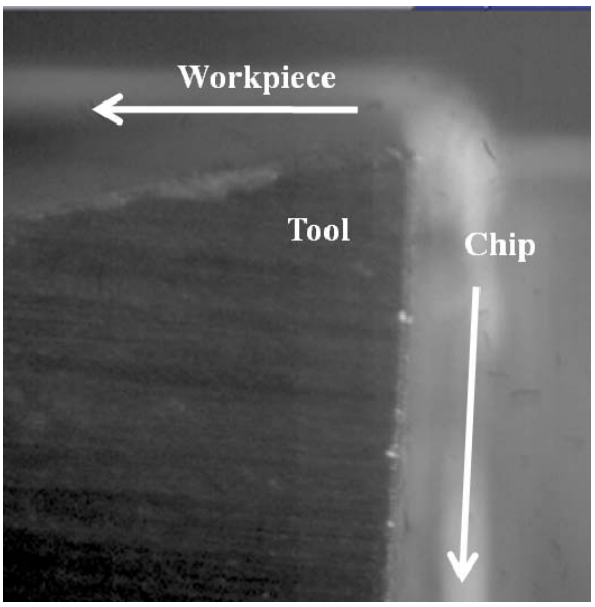

Figure 1. Visible Spectrum Camera Image – Side View of Orthogonal Cutting.

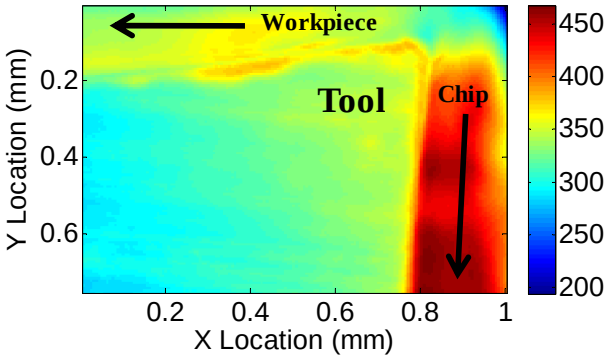

Figure 2. Infrared Spectrum Camera Image – Side View of Orthogonal Cutting. The Color Scale Indicates Radiance Temperature (°C)

EXPERIMENTAL RESULTS

In these experiments, a 3.6 mm thick, 125 mm diameter Ti-6Al-4V disk descends onto a cutting tool with a +6 degree rake angle and a flat rake face. The spindle and axis speeds result in an uncut chip thickness of 0.15 mm and cutting speeds between 55 m/min and 125 m/min. The configuration of the cameras provides an approximately 1.0 mm square field of view for the visible spectrum camera and an approximately 1.0 mm wide and 0.7 mm high field of view for the infrared camera. The visible spectrum camera acquired 256 pixel by 256 pixel video frames at

2 970 frames per second with 337 μs integration time. The infrared spectrum camera acquired 120 pixel by 160 pixel video frames at approximately 300 frames per second with 49 μs integration time. Performing all data acquisition at 2 megahertz enabled adequate synchronization of dynamometer data and video frame timings.

The measured cutting forces for each test provide the primary basis for selecting a time interval for processing measurement data and subsequent analysis. Figure 3 presents a representative example of the measured cutting forces as a function of time together with the tool temperature at a fixed location on the tool near the rake face. In these tests, the force and temperature data can be divided into three sections, an entry transient, a steady state, and an exit transient. As can be seen in Figure 3, the cutting forces ramp up, slightly overshoot the steady state level, and then converge to the steady state level in approximately one second. This convergence marks the transition between the entry transient and steady state sections of the test. During the entry transient, the tool temperature converges to the steady state level without overshooting. In the steady state region, the force and temperature measurements remain approximately constant for slightly less than one second. Finally, the forces decrease from the steady state level to zero in the exit transient portion of the test.

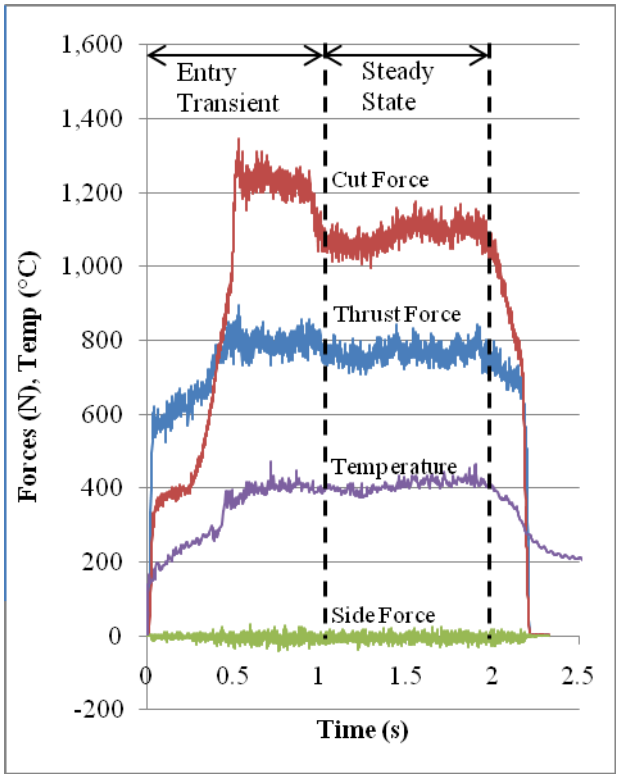

Figure 3. Measured Forces and Temperatures During an Orthogonal Cutting Test of Ti-6Al-4V at 55 m/min Cutting Speed and 0.15 mm feed.

For each test, observation of the visible spectrum video corresponding to the steady state section of the force data provides a basis for reducing the measurement uncertainty of the temperature data by ensuring the absence of visible disturbances. Due to the high magnification level employed, the camera lens must remain in very close proximity to the cutting tool. As a result, chips from the cutting process can strike the camera and cause it to move relative to the cutting edge. Also, portions of the chip can pass in front of the camera and obscure the camera field of view. Careful selection of the time interval for data analysis to avoid the appearance of these disturbances in the visible spectrum video data reduces measurement uncertainty.

Within the steady state region of the cutting force data in Figure 3, the time interval from 1.3 to 2.0 seconds provides a disturbance-free selection of data for subsequent analysis of the corresponding infrared video. The representative infrared video frame shown in Figure 2 occurs within the selected time interval. Prior to cutting, each insert was raised uniformly to 400 °C ± 10 °C (expanded uncertainty with a coverage factor k=2 [Taylor and Kuyatt 1994]), for 10 minutes to pre-oxidize the surface and stabilize emissivity. This treatment caused the exposed carbide to darken significantly. After treatment, a measured tool radiance temperature at a measured true temperature provides a basis for estimating a range for the tool surface emissivity of 0.8 ± 0.1 (k=2). The measured tool emissivity enables conversion of measured radiance temperatures to true temperatures using Wien's law [DeWitt and Nutter 1988]:

$$1/T_s = 1/T_\lambda + \lambda \ln(\varepsilon_\lambda)/c_2 \qquad (1)$$

where T_s and T_λ denote the true temperature and spectral radiance temperature (K), $\lambda = 4.35$ micrometers represents a weighted spectral wavelength determined through analysis of the camera's spectral response, c_2=14,387 mm·K is the second radiation constant, and $\varepsilon_\lambda = 0.8$ is the tool surface emissivity for spectral wavelength λ. Figure 4 presents the variation in measured true temperature at (X,Y) = (0.8 mm, 0.4 mm) in Figure 2 over the selected range of infrared video. As can be seen in Figure 4, the temperature fluctuates between approximately 375 °C and 450 °C, with an average true temperature of approximately 400 °C ± 25 °C (k=2). As configured for these experiments, the infrared camera measures infrared emissions over a spectral range from 3.8 μm to 5.1 μm. The use of the camera's full spectral range enables a shorter integration time of 49 μs, leading to a lower measurement uncertainty in the presence of significant variation due in part to the segmented chip formation in these experiments. The combined uncertainty includes contributions from emissivity variation of the tool surface, camera calibration, camera spectral response, the Wien's law approximation, material homogeneity, and optical effects, with emissivity variation as the dominant component [Whitenton 2010].

Averaging the measured temperatures for each pixel over the selected interval of infrared video frames provides a temperature profile of the tool similar to the individual frame in Figure 2, but with frame-to-frame variability as shown in Figure 4 removed. Figure 5 presents an example time-average true temperature profile of the cutting tool. It is important to note that the portions of Figure 5 that do not represent a point on the surface of the tool are masked since their emissivities differ substantially from those of the tool surface.

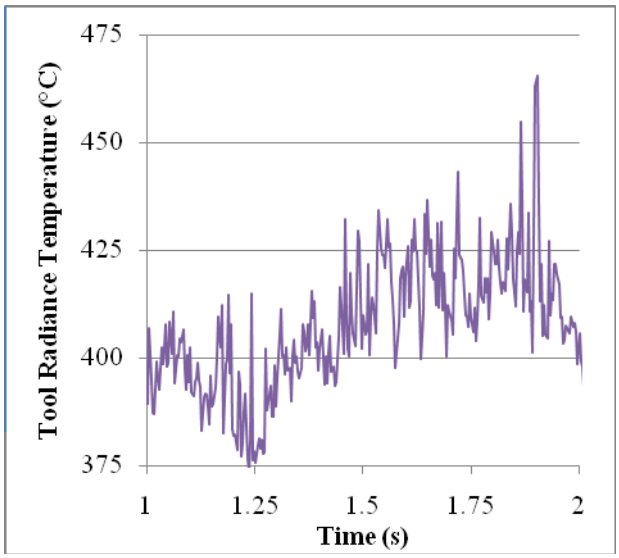

Figure 4. Measured True Temperature at Rake Face During Steady State.

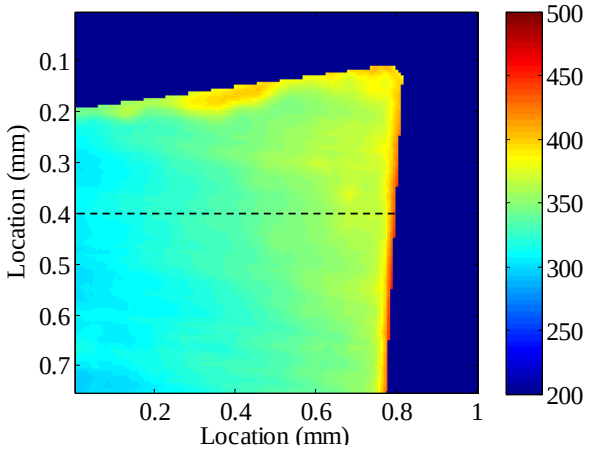

Figure 5. Distribution of True Temperatures (°C) in Cutting Zone – Averaged Over Selected Time Interval.

A quantitative comparison of full tool temperature distributions for different cutting conditions presents a significant difficulty in a static 2-dimensional figure. However, the pertinent characteristics of the temperature distribution can be extracted and compared with relative ease. A key example of this is the temperature along a horizontal line in the distribution that corresponds to the direction of the relative motion between the tool and the workpiece. Figure 6 presents an example profile of the measured true temperature of the cutting tool along the cutting direction at a vertical location that corresponds to the dashed line in Figure 5. The asterisk in Figure 6 indicates the approximate location of the rake face. As can be seen in Figure 6, a linear approximation of the tool temperature distribution along the cutting direction deviates from the measurement by less than 15 °C. Temperature distributions from different cutting tests through the same rake face location demonstrate strikingly similar localized deviations from linearity. While the actual true temperature profile is most likely not linear, the measurements support the hypothesis that the degree of nonlinearity is relatively small. Since the pattern of deviations appears highly repeatable from one test to the next, the most likely cause of the deviations is localized changes in surface emissivity.

A least-square linear fit of the measured data minimizes the sensitivity of the estimated rake face temperature to these local deviations when comparing measured profiles under different cutting conditions. Figure 7 presents linear fits to measured profiles for cutting at four different speeds with the same cutting tool (TiN-coated Tungsten Carbide) and workpiece material (Ti-6Al-4V). As can be seen in Figure 7, the peak tool true temperature increases from approximately 376 °C ± 25 °C to 444 °C ± 25 °C (k=2) as cutting speed increases from 55 m/min to 125 m/min.

The effect of cutting speed on the peak tool temperature should be considered in the context of corresponding changes in cutting forces. Converting the measured cutting forces into calculations of specific energies by dividing the measured force by the cross sectional area of the uncut chip provides a more generalized basis for comparing the results presented here with measurements made under other cutting conditions. The cross sectional area of the uncut chip is the width of the uncut chip, 3.59 mm, multiplied by the feed, 0.15 mm. Table 1 presents the resulting specific energies E_c (cutting energy) and E_t (thrust energy) together with the corresponding peak tool temperatures for four different cutting speeds with the Titanium Nitride (TiN) coated tool and for two different cutting speeds with an uncoated Tungsten Carbide (WC) tool. Figure 8 presents the temperatures and energies for the TiN coated tool. The specific cutting energy decreases slightly, while the specific thrust energy and peak tool temperature increase substantially. Comparing the temperatures and forces in Table 1 for the uncoated and coated tools at 90 m/min, the measured tool temperature for the uncoated tool is approximately 100 °C higher while the specific cutting and thrust energies are approximately 173 MPa and 505 MPa lower, respectively. At 55 m/min, the uncoated tool

temperature is approximately 80 °C higher and the specific cutting and thrust energies are approximately 90 MPa and 338 MPa lower, respectively. The increased temperatures and decreased specific cutting and thrust energies for the uncoated tool in comparison to the coated tool could be caused by a combination of increased friction on the rake face and increased thermal softening in the chip.

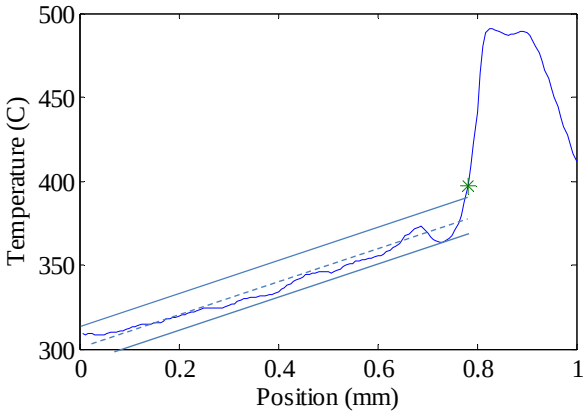

Figure 6. Measured True Temperature Distribution of the Tool in the Cutting Direction. Asterisk Indicates the Approximate Location of the Rake Face.

CONCLUSION

The high-speed infrared video based temperature measurement method for orthogonal cutting provides a sound platform for validation and benchmarking of machining models and simulations. The cutting tool temperatures, temperature profiles, and specific energies presented in this paper provide support for improving the confidence of the user community in machining modeling and simulation predictions. The observed dependence of the measured temperatures, temperature profiles, and forces on changes in surface speed provides a meaningful basis for evaluating the influence of material models, behavioral assumptions, and computational parameters on the resulting predictions.

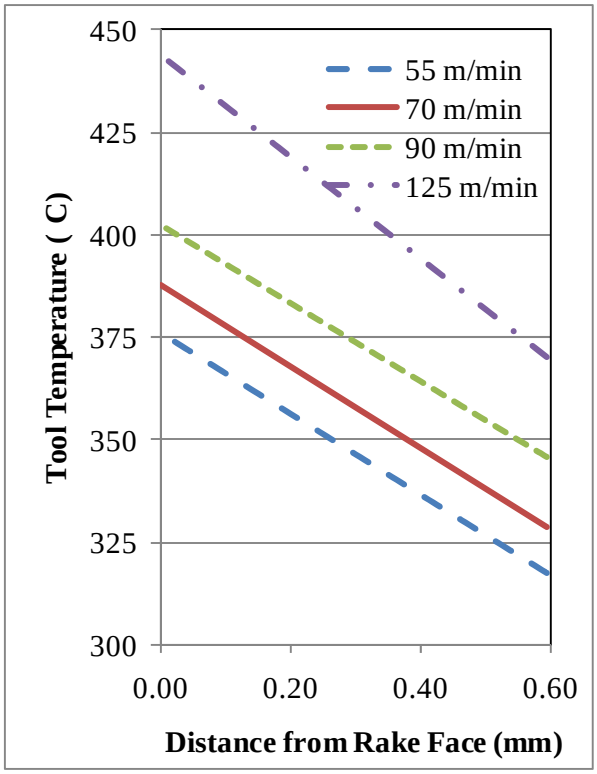

Figure 7. Effect of Cutting Speed on Tool Temperature Profile.

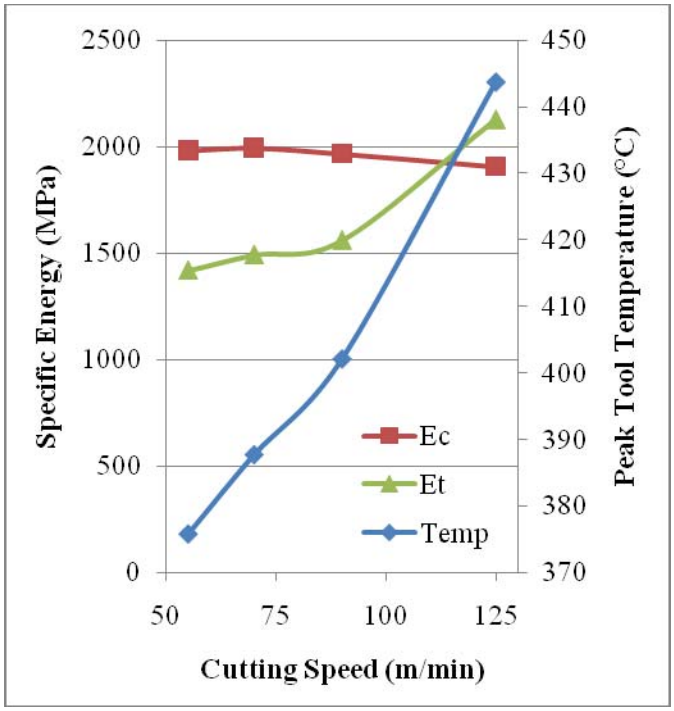

Figure 8. Effect of Cutting Speed on Peak (TiN-coated) Tool Temperature and Specific Energies.

Table 1. Measured Tool Temperatures and Specific Energies at Different Cutting Speeds (V_c).

V_c (m/min)	Temp (°C)	Ec (MPa)	Et (MPa)	Tool
55	376	1983	1419	TiN
70	388	1995	1492	TiN
90	402	1967	1560	TiN
125	444	1907	2126	TiN
55	457	1893	1082	WC
90	504	1794	1055	WC

ACKNOWLEDGEMENTS

The author acknowledges the support of Eric Whitenton, April Cooke, Alkan Donmez, and Hans Soons of the National Institute of Standards and Technology in the experimental research presented in this paper.

REFERENCES

Aluwihare CB, Armarego EJA, and Smith, AJR (2000) A Predictive Model for Temperature Distributions in 'Classical' Orthogonal Cutting, *Transactions of the North American Manufacturing Research Institution of SME* 28, 131-136.

Boothroyd, G (1961) Photographic Technique for the Determination of Metal Cutting Temperatures, *British Journal of Applied Physics* 12, 238-242.

Boston, OW, Gilbert, WW (1935) Cutting Temperatures Developed by Single-Point Turning Tools, *Trans. of the ASM* 23, 703-726.

Davies, MA, Yoon, H, Schmitz, TL, Burns, TJ and Kennedy, MD (2003) Calibrated thermal microscopy of the tool-chip interface in machining, *Journal of Machining Science and Technology* 7(2), 167-190.

Davies, MA, Cao, Q, Cooke, AL, Ivester, R (2003) On the Measurement and Prediction of Temperature Fields in Machining 1045 Steel, *CIRP Annals – Manufacturing Technology* 52(1),77-80.

Davies, MA, Ueda, T, M'saoubi, R, Mullany, B, Cooke, AL (2007) On the Measurement of Temperatures in Material Removal Processes, *CIRP Annals – Manufacturing Technology* 56(2), 581-604.

DeWitt, DP, and Nutter, GD (1988) *Theory and Practice of Radiation Thermometry*, Wiley-Interscience Publication, New York, NY.

Herbert, EG (1926) The Measurement of Cutting Temperatures, *Proceedings of the Institute of Mechanical Engineers*, 289-329.

Ivester, RW, Whitenton, E, Deshayes, L (2005) Comparison of Measurements and Simulations for Machining of Aluminum. *Transactions of the North American Manufacturing Research Institution of SME* 33, 429-436.

Komanduri, R (1993) Machining and Grinding: A Historical Review of the Classical Papers, *Applied Mechanics Reviews* 46(3) 80-129.

Stephenson, DA, (1993) Tool-Work Thermocouple Temperature Measurements – Theory and Implementation Issues, *ASME Journal of Engineering for Industry* 115, 432-437.

Stephenson, DA, and Agapiou, JS (1997) *Metal Cutting Theory and Practice*, Marcel Dekker, New York, NY.

Taylor, BN, and Kuyatt, CE (1994) Guidelines for Evaluating and Expressing the Uncertainty of NIST Measurement Results, National Institute of Standards and Technology Technical Note (TN) 1297.

Trigger, KJ (1948) Progress Report No. 1 on Tool-Chip Interface Temperatures, *Transactions of the ASME* 70, 91-98.

Trigger KJ, Chao BT (1951) An analytical evaluation of metal cutting temperatures. *ASME Transactions, Journal of Engineering for Industry* 73, 57-68.

Whitenton, E, Ivester, R, Yoon, H (2005) Simultaneous Visible and Thermal Imaging of Metals During Machining, *Proceedings of Thermosense*, Orlando, Florida.

Whitenton, E (2010) High-Speed Dual-Spectrum Imaging for the Measurement of Metal Cutting Temperatures, National Institute of Standards and Technology Interagency Report (NISTIR) 7650.